Acta Polytechnica **64**(5):455–463, 2024
https://doi.org/10.14311/AP.2024.64.0455

Published by the Czech Technical University in Prague

MODELLING AND ANALYSIS OF THREE-DIMENSIONAL CHEMICALLY REACTING, RADIATING CASSON-NANOFLUID FLOW: THERMOPHORESIS AND BROWNIAN MOTION EFFECTS

Poorna Kantha Tanuku[a], Lakshmi Prasanna Mamidi[b], Murali Gundagani[c,*]

[a] *Gayatri Vidya Parishad College of Engineering for Women, Department of Mathematics, Visakhapatnam, India*
[b] *Andhra University, Trans-Disciplinary Research Hub, Visakhapatnam, India*
[c] *Geethanjali College of Engineering and Technology, Department of Mathematics, Cheeryal, India*
[*] corresponding author: muraligundagani@gmail.com

Abstract. In the presence of a porous material and a magnetic field, the authors of this work must evaluate the combined effects of chemical reaction and thermal radiation on a Casson-nanofluid flow in three dimensions towards a linearly stretched sheet. Using the Roseland approximation, which integrates the effect of thermal radiation into the energy equation, thermal radiation is included in this study. The governing equation with initial and boundary conditions is converted to dimensionless form by adding pertinent non-dimensional variables and parameters, and then numerically solved using the finite element method. The effects of key variables on velocity, temperature, and concentration are shown graphically, followed by tabular representations of the effect of these parameters on skin friction, Nusselt, and Sherwood numbers and an in-depth explanation. This is essential for several technological applications, such as oil heat recovery, termite welding, transpiration cooling, and drag reduction. A comparison of our numerical results with previously published data reveals a high degree of agreement between the two sets of information. This new research has implications for energy systems, biomedical engineering and aeronautics, and has significant implications for the food industry.

Keywords: MHD chemical reaction, three-dimensional Casson fluid, nanofluid, linear stretching sheet thermal radiation, porous medium, finite element technique.

1. Introduction

Flow through stretched films is critical to several engineering and industrial processes, such as metal spinning, plastic film stretching, glass blowing, crystal development, and filament cooling. The speed at which the plate is stretched has a significant influence on the quality of the final product. The problem of 2-dimensional boundary layer flow over elongated surfaces was first identified by Crane [1]. A study by Waini et al. [2] on hybrid nanofluid flow induced by exponential expansion and contraction of radiation and Magneto hydrodynamics sensitive layers. The effect of exponentially expanding surfaces on nanoliquid flow via viscous dissipation has been reviewed in [3, 4]. The effect of the suction parameter on the negative velocity profile of micropolar liquid flow through non-isothermally exponentially expanding layers was demonstrated by Mandal and Mukhopadhyay [5]. In a study [6], Subhani and Nadeem investigated normal and hybrid nanofluidic flows generated by exponentially growing surface theory. Radiative magneto-hydrodynamic flux through a permeable stretched surface absorbed in a porous medium was observed by Agrawal et. al. [7] using the fourth-order Runga-Kutta technique. The impact of repetitive sliding and angular magnetic fields on the flow of hybrid nanofluids across nonlinearly stretched sheets was reported by Abbas et al. [8]. Aly and Pop [9] compared their hybrid nanofluids with conventional nanofluids in terms of stagnation point MHD flow occurring in expanding/contracting membranes.

Chaudhary and Kanika [10] studied how thermal radiation and heat generation/absorption affect the contraction/expansion flux of permeable nanoliquids on heated foils at MHD stagnation points. Poldanjani et al. [11] studied how thermal radiation and magnetic fields affect entropy enhancement when heat is transferred from a nanoliquid moving inside a cavity. Sheikholeslami [12] studied how magnetic fields and heat from the environment affect the thermal convection between two layers of flowing nanoliquids. Mahantesh et al. [13] studied a magnetohydrodynamic nanofluid flow with a nonlinear strain foil-induced slip in three dimensions within the existence of thermal radiation and mixed convection. Sedki et al. [14] studied the effect of radiative heat of boundary layer flow on unstable mixed convection of nanoliquids across permeable and stretchable surfaces in porous media under exothermic conditions. Xenos et al. [15] studied how changes in radiation and pressure affect the fluid flow in a nonlinear boundary layer on a flat plate. Aly and Ebaid [16] studied the boundary layer Marangoni MHD problem used for nanofluidic hybrids

with radiant heat. Sankaran et al. [17] considered how thermal radiation affects the pressure flow of nanofluidic copper water between comparable plates. Ramesh et al. [18] studied Casson's nanofluidic flow and Maxwellian fluid flow that occur when a surface is stretched.

The emergence of new species during chemical reactions in nanofluidic flows will greatly affect the motion of objects, resulting in changing production requirements. Eid, Chamkha and Makinde [19, 20] used Joule heating and species reactions to study the impact of solar radiation based on the convection of MHD nanofluids across stretched sheets in porous media. M.D. Shamshuddin et al. [21] studied the thermal and solutal performance of Cu/CuO nanoparticles on a non-linear radially stretching surface.

M. C. Krishna Reddy et al. [22] studied heat and mass transfer effects on unsteady MHD free convection flow past a vertical permeable moving plate with radiation. G. Murali et al. [23] analysed Heat and mass transfer effects on an unsteady hydromagnetic free convective flow over an infinite vertical plate embedded in a porous medium with heat absorption. Deepa Gadipally et al. [24] carried out an analysis of Soret and Dufour effects on unsteady MHD flow past a semi-infinite vertical porous plate using finite difference method. Murali et al. [25] found the impact of chemical reaction effects on unsteady MHD fluid flow past an infinite vertical plate embedded in a porous medium with a variable suction. N. V. N. Babu et al. [26] analysed Soret and Dufour effects on unsteady hydromagnetic free convective fluid flow past an infinite vertical porous plate in the presence of a chemical reaction. The finite element solutions for MHD-driven problem solving system were given by [27, 28]. The works mentioned in the literature [29–35] had a significant impact on understanding the nature of this study, which is a continuation of Nadeem et al. [36].

Calculated flow variables, such as velocity, temperature, and concentration profiles are displayed in tables and graphs for various physical components. This new research has implications for energy systems, biomedical engineering, and aeronautics, and has significant implications for the food industry.

2. Mathematical formulation

This article presents the steady, conductive, incompressible, magnetohydrodynamic three-dimensional flow of Casson nanofluids in the presence of thermophoresis, Brownian motion, thermal radiation, chemical reactions, porous media, and chemical reaction effects. Figure 1 shows the physical coordinate system and the geometry of this problem for this flow.

(1.) Define the velocity component along the (x, y, z) direction as (u, v, w).

(2.) The flow is generated by an ever-expanding surface.

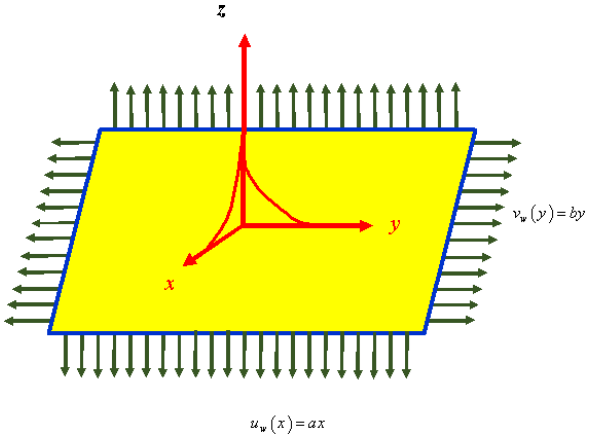

Figure 1. Geometrical illustration of Nano-Casson fluid flow.

(3.) A uniform magnetic field of strength B_0 is to be relevant in the direction of Z.

(4.) The magnetic Reynolds number is supposed to be very low and the induced magnetic field is derelict.

(5.) Brownian motion and thermophoresis are taken into account.

(6.) The rheological equation for non-Newtonian fluids is described as:

$$\tau = \tau_0 + \mu\alpha^*. \tag{1}$$

For Casson fluid, Equation (1) may be extended as:

$$\begin{aligned} \tau_{ij} &= 2\left(\mu_B + \frac{p_y}{\sqrt{2\pi}}\right)e_{ij}, \\ \pi > \pi_c \;\&\; & 2\left(\mu_B + \frac{p_y}{\sqrt{2\pi_c}}\right)e_{ij}, \\ \pi < \pi_c, & \end{aligned} \tag{2}$$

where

$\pi = e_{ij}e_{ji}$ with e_{ij} is the $(i,j)^{\text{th}}$ component of the fluid deformation rate,

$p_y = \frac{\mu_B\sqrt{2\pi}}{\beta}$ is the yield stress of the Casson fluid.

For this flow, the governing boundary layer equations can be written as:

- Equation of continuity:

$$\frac{\partial u}{\partial x} + \frac{\partial v}{\partial y} + \frac{\partial w}{\partial z} = 0. \tag{3}$$

- Momentum equation:

$$\begin{aligned} &u\left(\frac{\partial u}{\partial x}\right) + v\left(\frac{\partial u}{\partial y}\right) + w\left(\frac{\partial u}{\partial z}\right) \\ &= \nu\left(1 + \frac{1}{\beta}\right)\left(\frac{\partial^2 u}{\partial z^2}\right) - \left(\frac{\nu}{k^*}\right)u - \left(\frac{\sigma B_o^2}{\rho}\right)u, \end{aligned} \tag{4}$$

$$\begin{aligned} &u\left(\frac{\partial v}{\partial x}\right) + v\left(\frac{\partial v}{\partial y}\right) + w\left(\frac{\partial v}{\partial z}\right) \\ &= \nu\left(1 + \frac{1}{\beta}\right)\left(\frac{\partial^2 v}{\partial z^2}\right) - \left(\frac{\nu}{k^*}\right)v - \left(\frac{\sigma B_o^2}{\rho}\right)v. \end{aligned} \tag{5}$$

- Equation of thermal energy:

$$u\left(\frac{\partial T}{\partial x}\right)+v\left(\frac{\partial T}{\partial y}\right)+w\left(\frac{\partial T}{\partial z}\right)=\alpha\left(\frac{\partial^2 T}{\partial z^2}\right)+\tau_1\left\{D_B\left(\frac{\partial T}{\partial z}\right)\left(\frac{\partial \varphi}{\partial z}\right)+\frac{D_T}{T_\infty}\left(\frac{\partial T}{\partial z}\right)^2\right\}-\frac{1}{\rho C_p}\left(\frac{\partial q_r}{\partial z}\right), \tag{6}$$

- Equation of species concentration:

$$u\left(\frac{\partial \varphi}{\partial x}\right)+v\left(\frac{\partial \varphi}{\partial y}\right)+w\left(\frac{\partial \varphi}{\partial z}\right)=D_B\left(\frac{\partial^2 \varphi}{\partial z^2}\right)+\frac{D_T}{T_\infty}\left(\frac{\partial T}{\partial z}\right)^2-\mathrm{Kr}(\varphi-\varphi_w). \tag{7}$$

The boundary conditions for this flow are:

$$\begin{cases} u=u_w(x)=ax,\ v=v_w(y)=by, \\ T=T_w,\ \varphi=\varphi_w \\ u\to 0,\ v\to 0,\ T\to T_\infty, \\ \varphi\to\varphi_\infty \end{cases} \begin{array}{l} \text{at } z=0, \\ \\ \text{as } z\to\infty. \end{array} \tag{8}$$

We have used the Rosseland approximation for radiation:

$$q_r=-\frac{2^2\sigma^*}{3K^*}\left(\frac{\partial T^4}{\partial z}\right). \tag{9}$$

Suppose there is a temperature difference in the flow, we expand T^4 in a Taylor series on T_∞, as given below:

$$T^4=T_\infty^4+4\,(T-T_\infty)\,T_\infty^3+6\,(T-T_\infty)^2\,T_\infty^2+\ldots. \tag{10}$$

If the terms of higher order are ignored, we obtain:

$$T^4\cong 2^2TT_\infty^3-3T_\infty^3. \tag{11}$$

Thus replacing Equation (11) in Equation (9), we find:

$$q_r=-\frac{16T_\infty^3\sigma^*}{3K^*}\left(\frac{\partial T}{\partial z}\right). \tag{12}$$

Using (8), Equation (3) can be written as:

$$u\left(\frac{\partial T}{\partial x}\right)+v\left(\frac{\partial T}{\partial y}\right)+w\left(\frac{\partial T}{\partial z}\right)=\alpha\left(\frac{\partial^2 T}{\partial z^2}\right)+\tau_1\left\{D_B\left(\frac{\partial T}{\partial z}\right)\left(\frac{\partial \varphi}{\partial z}\right)+\frac{D_T}{T_\infty}\left(\frac{\partial T}{\partial z}\right)^2\right\}+\frac{1}{\rho C_p}\left(\frac{16T_\infty^3\sigma^*}{3K^*}\right)\left(\frac{\partial^2 T}{\partial z^2}\right). \tag{13}$$

Let us introduce these similarity transformations:

$$\left.\begin{array}{l} u=a\,(x+y)\,f'(\eta), \\ v=b(x+y)g'(\eta),\ w=-\sqrt{a\nu}\{f(\eta)+Cg(\eta)\}, \\ \eta=\left(\sqrt{\frac{a}{\nu}}\right)z,\ \theta=\frac{T-T_\infty}{T_w-T_\infty},\ \phi=\frac{\varphi-\varphi_\infty}{\varphi_w-\varphi_\infty}. \end{array}\right\} \tag{14}$$

Using Equation (14), the equation of continuity is identically contented and Equations (4), (5), (7), and (13) become:

$$\left(1+\frac{1}{\beta}\right)f'''+f''f+f''g-f'^2-f'(\lambda+M)=0, \tag{15}$$

$$\left(1+\frac{1}{\beta}\right)g'''+fg''+gg''-g'^2-(M+\lambda)g'=0, \tag{16}$$

$$\left(1+\frac{4R}{3}\right)\theta''+Prf\theta'+Prg\theta'+PrNb\theta'\phi'+PrNt\theta'^2=0, \tag{17}$$

$$\mathrm{Nb}\,\phi''+\mathrm{Nb}\,\mathrm{Sc}f\phi'+\mathrm{Nb}\,\mathrm{Sc}g\phi'+\mathrm{Nt}\,\theta''-\mathrm{Sc}\,\mathrm{Nb}\,\gamma\phi=0, \tag{18}$$

the corresponding boundary conditions (8) become:

$$\left.\begin{array}{l} f(0)=0,\ g(0)=0,\ f'(0)=1, \\ g'(0)=C,\ \theta(0)=1,\ \phi(0)=1, \\ f'(\infty)\to 0,\ g'(\infty)\to 0, \\ \theta(\infty)\to 0,\ \phi(\infty)\to 0. \end{array}\right\} \tag{19}$$

The following are the physical parameters:

$$\left.\begin{array}{l} M=\frac{\sigma B_o^2}{\rho a},\ R=\frac{4\sigma^*T_\infty^3}{\kappa K^*}, \\ \mathrm{Nb}=\frac{\tau_1 D_B(\varphi_w-\varphi_\infty)}{\nu},\ \mathrm{Pr}=\frac{\nu}{\alpha}, \\ \mathrm{Nt}=\frac{\nu D_T(T_w-T_\infty)}{\nu T_\infty},\ C=\frac{b}{a}, \\ \mathrm{Sc}=\frac{\nu}{D_B},\ \lambda=\frac{1}{ak^*}. \end{array}\right\} \tag{20}$$

The quantities of physical interest, the physical parameters of the skin friction coefficient Cf, along the X and Y directions, and the local Nusselt number are listed below:

$$\mathrm{Cf}_x=\frac{\tau_{wx}}{\rho u_w^2}\Rightarrow\left(\sqrt{\mathrm{Re}_x}\right)\mathrm{Cf}_x=\left(1+\frac{1}{\beta}\right)f''(0), \tag{21}$$

$$\mathrm{Cf}_y=\frac{\tau_{wy}}{\rho u_w^2}\Rightarrow\left(\sqrt{\mathrm{Re}_y}\right)\mathrm{Cf}_y=\left(1+\frac{1}{\beta}\right)g''(0), \tag{22}$$

$$\mathrm{Nu}_x=\frac{xq_w}{\kappa(T_w-T_\infty)}=-\frac{x\left(\frac{\partial T}{\partial z}+\frac{\partial q_r}{\partial z}\right)_{z=0}}{\kappa(T_w-T_\infty)} \Rightarrow \mathrm{Nu}_x=-\left(1+\frac{4R}{3}\right)\left(\sqrt{\mathrm{Re}_x}\right)\theta'(0), \tag{23}$$

$$\mathrm{Sh}=\frac{xq_m}{D_B(\varphi_w-\varphi_\infty)}=-\frac{x\left(\frac{\partial \varphi}{\partial y}\right)_{y=0}}{D_B(\varphi_w-\varphi_\infty)} \Rightarrow \mathrm{Sh}=-\left(\sqrt{\mathrm{Re}_x}\right)\phi'(0), \tag{24}$$

$$\mathrm{Re}_x=\frac{u_x(x)x}{\nu}, \tag{25}$$

$$\mathrm{Re}_y=\frac{v_w(y)y}{\nu}. \tag{26}$$

On the basis of the stretching velocities, above local Reynolds numbers (25) and (26) are shown.

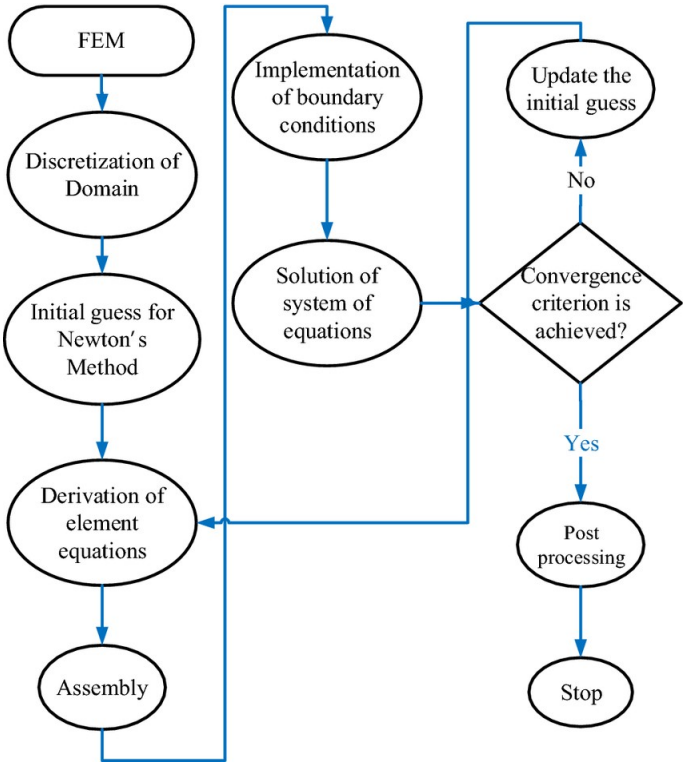

Figure 2. FEM flow chart.

3. Method of solution

The finite element method employed in the current study can be used in future research since it is a highly useful approach to solving linear and nonlinear partial and ordinary differential equations in physics, mechanical engineering, and other related fields. This was the most adaptable numerical technique available at the time this article was written for carrying out an engineering analysis. Numerous numerical techniques, including the LU decomposition approach, the Gauss elimination method, and others, can be used to solve the equations.

The idea that the problem domain can be segmented into smaller, more manageable chunks that also have limited dimensions and are referred to as "finite elements" is the driving idea behind the finite element approach. This idea was inspired by the fact that these chunks can be broken down into smaller, more manageable chunks. It has been put to use in the attempt to provide an explanation for a broad variety of occurrences, including the transmission of heat, the mechanics of fluids and solids, the dynamics of rigid bodies, the mechanics of solids, chemical processes, electrical systems, and acoustics. The use of the finite element approach is shown in Figure 2, which also serves as an example.

Before one can carry out a finite element analysis, it is required to finish the phases that are listed below, which are as follows:

- discretisation of the domain into elements,
- elementation of the domain,
- constructing equations and determining the answers to those equations,
- imposing boundary conditions.

The solution of differential equations is one of the most popular uses for these approaches. When working with real numbers, it is necessary to bear in mind that the form functions can be used to provide a close approximation of real functions. If you follow this technique step by step, you can be certain that your calculations will be accurate. The flow domain has a total of 20 001 nodes and is divided into 10 000 quadratic components that are of the same size and shape. The flow domain consists of 10 000 quadratic components, all of which are of the same magnitude as their counterparts in the other components. After the element equations were developed, there were a total of 80 004 nonlinear equations that could be investigated. These equations were made accessible for the study.

After the boundary conditions have been applied, the Gauss approach is applied to remove the remaining system of nonlinear equations, and then the Gauss technique is used to arrive at a numerical solution that is accurate to 0.00001 degrees. The use of Gaussian quadrature is done to help with the challenges associated with integration.

The method's custom software was run on a desktop computer within the context of a suitable programming environment. The software was developed specifically for the method. MATHEMATICA is the name of the programming language that was used to create the software application for the computer.

λ	Present $\left(1+\frac{1}{\beta}\right) f''(0)$	Nadeem et al. [36] $\left(1+\frac{1}{\beta}\right) f''(0)$	Present $\left(1+\frac{1}{\beta}\right) g''(0)$	Nadeem et al. [36] $\left(1+\frac{1}{\beta}\right) g''(0)$
0.0	1.5309316847983463	1.5459	0.6367890798398319	0.6579
0.5	1.8088818378637911	1.8361	0.8097718346039391	0.8228
1.0	2.0696782733471607	2.0884	0.9478196983091393	0.9614

TABLE 1. Assessment of obtained skin-friction results with published results of Nadeem et al. [36] when $R = \mathrm{Nb} = \mathrm{Nt} = \mathrm{Pr} = \mathrm{Sc} = \gamma = 0$, $C = 0.5$ and $\beta = 1.0$.

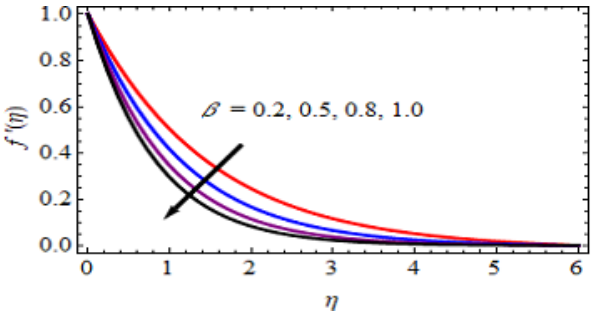

FIGURE 3. Impact of β on $f'(\eta)$.

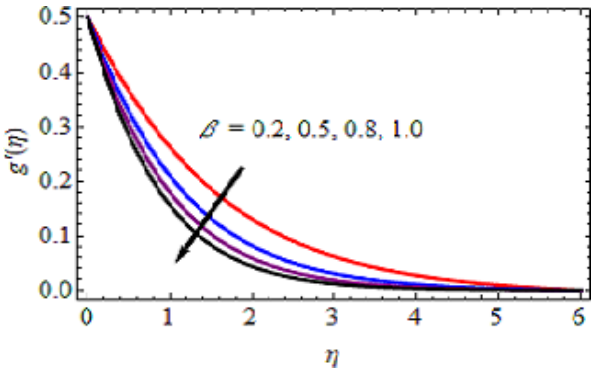

FIGURE 4. Behaviour of β on $g'(\eta)$.

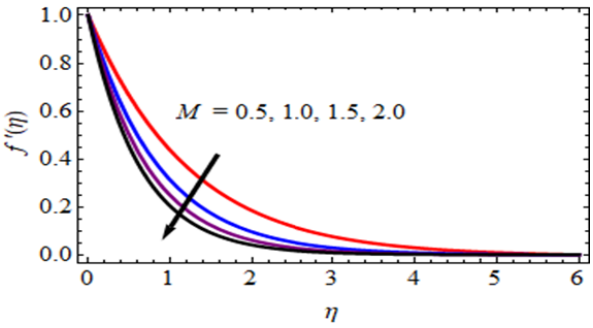

FIGURE 5. Sequel of M on velocity profiles.

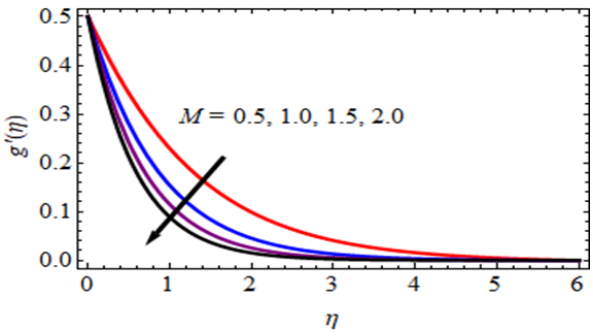

FIGURE 6. Behaviour of M on $g'(\eta)$.

Program code validation In the absence of thermal radiation, Prandtl number, thermophoresis, Brownian motion, Schmidt number, and chemical reaction effects, the authors have compared the obtained skin friction results with the published results of Nadeem et. al. [29] used for the variations of permeability parameter at $C = 0.5$ and $\beta = 1.0$ in Table 1, which shows a good agreement.

4. RESULTS AND DISCUSSION

Figures 3 and 4 illustrate the influence of non-Newtonkason fluid parameters β on the first and second order velocity profiles. Here we see that increasing the non-Newton-Kasson fluid parameter β creates resistance to fluid flow. The result is as shown in the picture. Figures 3 and 4: Higher values of the non-Newtonian Casson fluid parameter β decrease the magnitude of the first and second order velocity profiles and the thickness of the boundary layer. Non-Newtonian Casson fluid parameter β increases to infinity and the current phenomenon in Newtonian fluids decreases significantly.

As shown in Figures 5 and 6, rising the magnetic field parameter (M) decreases both the thickness of the boundary layer and the magnitude of the primary and secondary velocity profiles. Physically, the electric current phenomenon takes place as a magnetic field induces an electric current in a conducting liquid, exerting a drag force on the liquid at the interface and slowing it down. From this we can conclude that a magnetic field is present.

According to Figures 7 and 8, the first and second order velocity profiles decrease as the value of the porosity parameter λ in the boundary layer increases. Furthermore, Figures 7 and 8 show that the boundary layer thickness decreases as λ increases.

Figure 9 illustrates the influence of the stretch ratio parameter C on the quadratic velocity profile. The quadratic velocity profile is increased by increasing the value of the stretch rate ratio C parameter. In general, increasing the strain parameter C increases the yield pressure. Figure 10 shows the impact of the Prandtl number Pr on the liquid temperature. As the Prandtl number Pr increases, the liquid temperature gradient decreases. A liquid with a high Prandtl number has

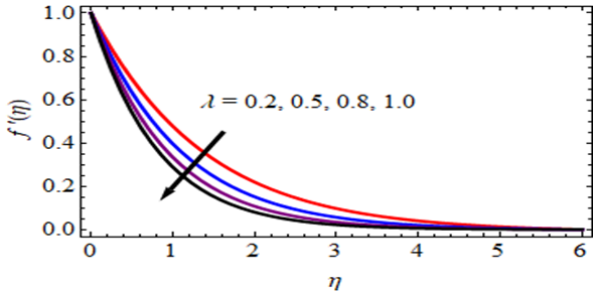

Figure 7. Behaviour of λ on $f'(\eta)$.

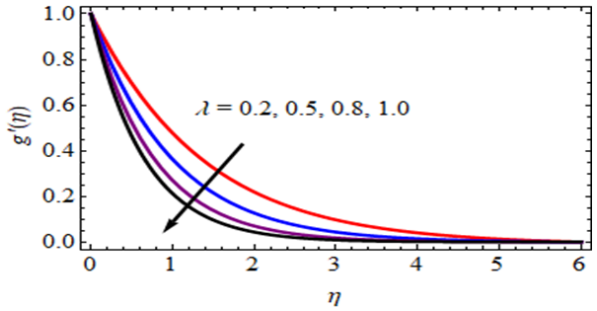

Figure 8. Impact of λ on $g'(\eta)$.

a low thermal conductivity, and therefore a lower temperature. This figure demonstrates the impact of the radiation parameter R on the temperature profile. If the heat dissipation parameter R is greater than the standard value, the temperature rises. As R increases, the thermal buoyancy increases, but the thickness of the thermal boundary layer decreases. Increasing the heat radiation parameter R generates more heat in the fluid flow zone, resulting in a more uniform temperature profile.

Figure 11 demonstrates the influence of the thermal radiation parameter R on the temperature profile. This graph clearly shows that the temperature increases as the radiation parameter increases. This is because an increase in thermal radiation has the effect of thermal energy being released into the liquid.

Figures 12 and 13 demonstrate the influence of the Brownian motion parameter Nb on the temperature and concentration profiles. Increasing the Brownian motion parameter Nb in Figure 12 improves the temperature profile. As shown in Figure 12, the larger the Brownian motion parameter, the smaller the viscous force, and the larger the Brownian diffusion coefficient, the larger the thickness and temperature of the thermal boundary layer. As shown in Figure 13, the concentration decreases as the Nb concentration increases.

The effect of thermophoretic parameters Nt on the temperature and concentration profiles is shown in Figures 14 and 15. Thermal diffusion coefficients and viscous forces influence thermophoretic parameters. Since the viscous force is inversely proportional to Nt, an increase in Nt implies a decrease in viscous force and an increase in the thermal diffusion coefficient with the increase of temperature and nanoparticle concentration.

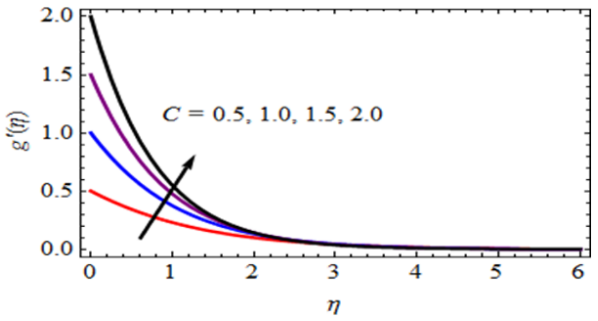

Figure 9. Sequel of C on $g'(\eta)$.

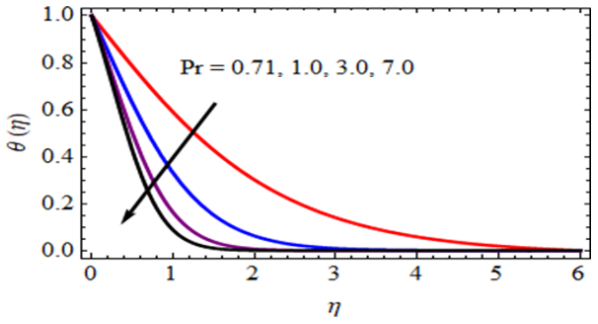

Figure 10. Performance of Pr on $\theta(\eta)$.

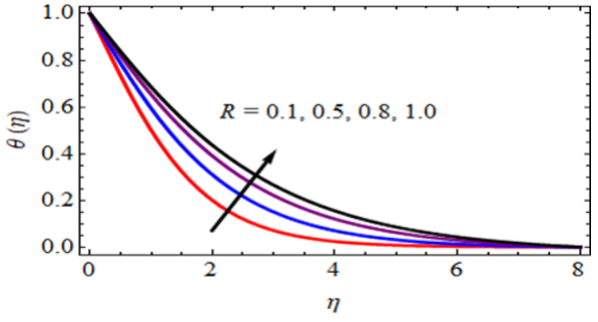

Figure 11. Behaviour of R on $\theta(\eta)$.

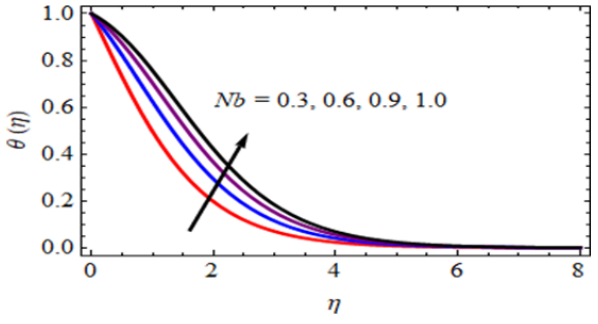

Figure 12. Analyse of Nb on $\theta(\eta)$.

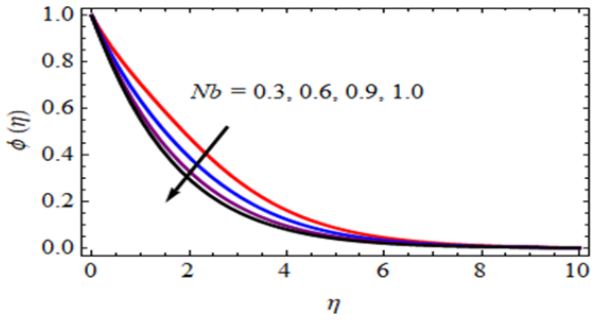

Figure 13. Behaviour of Nb on $\phi(\eta)$.

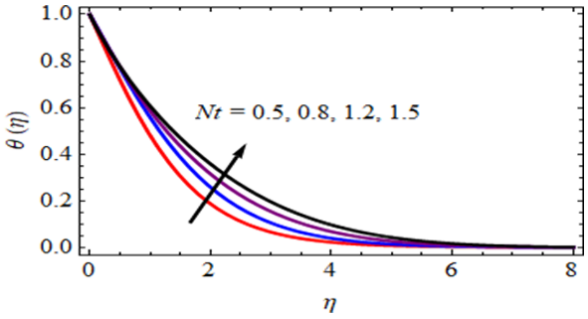

FIGURE 14. Behaviour of Nt on $\theta(\eta)$.

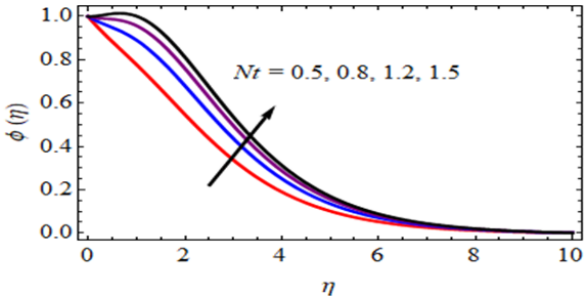

FIGURE 15. Impact of Nt on $\phi(\eta)$.

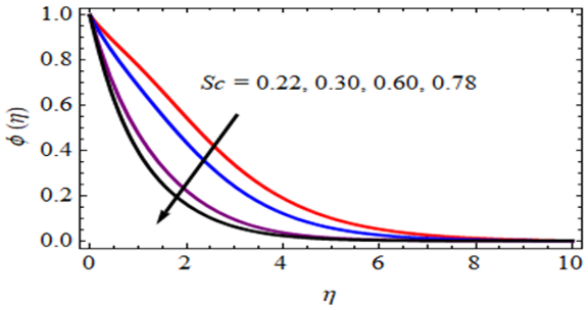

FIGURE 16. Impact of Sc on $\phi(\eta)$.

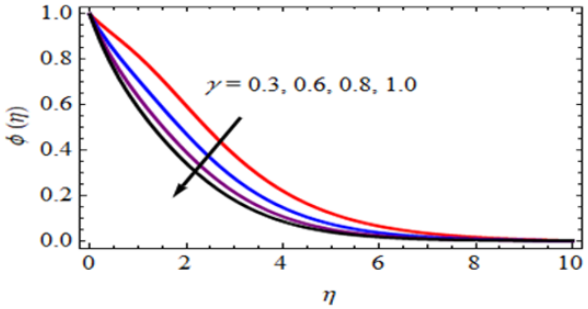

FIGURE 17. Impact of γ on $\phi(\eta)$.

The influence of the Schmidt number (Sc) on the concentration profile is shown in Figure 16. Sc represents the momentum-to-mass diffusivity ratio, and the diffusion in the concentration (species) boundary layer is used to determine the relative values of momentum and mass transfer. As Sc increases, the mass diffusivity of the liquid decreases, resulting in lower $\varphi(\eta)$. Since the mass diffusivity and Sc are inversely related, a higher Sc value correlates to a weaker concentration interface. Figure 17 explains the influence of the chemical reaction parameter γ on the concentration profile.

5. Conclusion

This paper presented the effect of thermal radiation and chemical reaction on three-dimensional, steady, viscous, incompressible, viscous, electrically conducting Casson-nanofluid flow towards a linearly stretching sheet through a porous medium in the presence of thermophoresis and Brownian motion effects. The basic governing equations of the flow are solved numerically using a finite element technique. An extensive numerical parametric study is carried out on the numerical explanation of a class of nonlinear equations to describe the details of the solution and results are detailed in the form of graphs. The resulting conclusions are:

- All velocity profiles decreased as the Casson fluid parameter, the magnetic field parameter, and the permeability parameter increased.
- The temperature profile increased as the thermal radiation, thermophoretic, and Brownian motion parameters increased while the Prandtl number decreased.
- Concentration profiles decreased as the Schmidt number, Brownian motion parameters, and chemical reaction parameters increased, while thermophoretic parameters increased the concentration profile.
- The thickness of the mass transfer velocity boundary layer decreases with increasing Brownian motion parameters, Schmidt numbers, chemical reaction parameters, and thermophoretic parameters.
- Finally, we compare the current findings with those of Nadeem et al. [36] for limited values of these parameters.
- Apart from that, the results indicate that the proposed method is appropriate for solving the current problems.

References

[1] L. J. Crane. Flow past a stretching plate. *Zeitschrift für angewandte Mathematik und Physik ZAMP* **21**(4):645–647, 1970. https://doi.org/10.1007/BF01587695

[2] I. Waini, A. Ishak, I. Pop. Hybrid nanofluid flow induced by an exponentially shrinking sheet. *Chinese Journal of Physics* **68**:468–482, 2020. https://doi.org/10.1016/j.cjph.2019.12.015

[3] N. A. Zainal, R. Nazar, K. Naganthran, I. Pop. Viscous dissipation and MHD hybrid nanofluid flow towards an exponentially stretching/shrinking surface. *Neural Computing and Applications* **33**(17):11285–11295, 2021. https://doi.org/10.1007/s00521-020-05645-5

[4] A. S. Rao, K. D. Ramaiah, G. Kotha, et al. A spectral relaxation approach for boundary layer flow of nanofluid past an exponentially stretching surface with variable suction in the presence of heat source/sink with viscous dissipation. *Arabian Journal for Science and*

Engineering **46**(8):7509–7520, 2021.
https://doi.org/10.1007/s13369-021-05422-z

[5] I. C. Mandal, S. Mukhopadhyay. Nonlinear convection in micropolar fluid flow past a non-isothermal exponentially permeable stretching sheet in presence of heat source/sink. *Thermal Engineering* **67**(4):202–215, 2020. https://doi.org/10.1134/S0040601520040059

[6] M. Subhani, S. Nadeem. Numerical analysis of micropolar hybrid nanofluid. *Applied Nanoscience* **9**(4):447–459, 2019.
https://doi.org/10.1007/s13204-018-0926-2

[7] P. Agrawal, P. K. Dadheech, R. N. Jat, D. Baleanu. Radiative MHD hybrid-nanofluids flow over a permeable stretching surface with heat source/sink embedded in porous medium. *International Journal of Numerical Methods for Heat & Fluid Flow* **31**(8):2818–2840, 2021.
https://doi.org/10.1108/HFF-11-2020-0694

[8] N. Abbas, S. Nadeem, A. Saleem, et al. Models base study of inclined MHD of hybrid nanofluid flow over nonlinear stretching cylinder. *Chinese Journal of Physics* **69**:109–117, 2021.
https://doi.org/10.1016/j.cjph.2020.11.019

[9] E. H. Aly, I. Pop. MHD flow and heat transfer near stagnation point over a stretching/shrinking surface with partial slip and viscous dissipation: Hybrid nanofluid versus nanofluid. *Powder Technology* **367**:192–205, 2020.
https://doi.org/10.1016/j.powtec.2020.03.030

[10] S. Chaudhary, K. M. Kanika. Heat generation/absorption and radiation effects on hydromagnetic stagnation point flow of nanofluids toward a heated porous stretching/shrinking sheet with suction/injection. *Journal of Porous Media* **23**(1):27–49, 2020.
https://doi.org/10.1615/JPorMedia.2019026922

[11] A. Hajatzadeh Pordanjani, S. Aghakhani, A. Karimipour, et al. Investigation of free convection heat transfer and entropy generation of nanofluid flow inside a cavity affected by magnetic field and thermal radiation. *Journal of Thermal Analysis and Calorimetry* **137**(3):997–1019, 2019.
https://doi.org/10.1007/s10973-018-7982-4

[12] M. Sheikholeslami. Numerical simulation of magnetic nanofluid natural convection in porous media. *Physics Letters A* **381**(5):494–503, 2017.
https://doi.org/10.1016/j.physleta.2016.11.042

[13] B. Mahanthesh, B. J. Gireesha, R. S. R. Gorla, O. D. Makinde. Magnetohydrodynamic three-dimensional flow of nanofluids with slip and thermal radiation over a nonlinear stretching sheet: A numerical study. *Neural Computing and Applications* **30**(5):1557–1567, 2018.
https://doi.org/10.1007/s00521-016-2742-5

[14] A. M. Sedki, S. M. Abo-Dahab, J. Bouslimi, K. H. Mahmoud. Thermal radiation effect on unsteady mixed convection boundary layer flow and heat transfer of nanofluid over permeable stretching surface through porous medium in the presence of heat generation. *Science Progress* **104**(3):00368504211042261, 2021.
https://doi.org/10.1177/00368504211042261

[15] M. A. Xenos, E. N. Petropoulou, A. Siokis, U. S. Mahabaleshwar. Solving the nonlinear boundary layer flow equations with pressure gradient and radiation. *Symmetry* **12**(5):710, 2020.
https://doi.org/10.3390/sym12050710

[16] E. H. Aly, A. Ebaid. MHD marangoni boundary layer problem for hybrid nanofluids with thermal radiation. *International Journal of Numerical Methods for Heat & Fluid Flow* **31**(3):897–913, 2021.
https://doi.org/10.1108/HFF-05-2020-0245

[17] S. Sivasankaran, M. Bhuvaneswari, T. Chandrapushpam, S. Karthikeyan. Influence of thermal radiation on squeezing flow of copper-water nanofluid between parallel plates. *Materials Today: Proceedings* **42**:457–464, 2021.
https://doi.org/10.1016/j.matpr.2020.10.184

[18] G. K. Ramesh, B. C. Prasannakumara, B. J. Gireesha, et al. Three dimensional flow of Maxwell fluid with suspended nanoparticles past a bidirectional porous stretching surface with thermal radiation. *Thermal Science and Engineering Progress* **1**:6–14, 2017.
https://doi.org/10.1016/j.tsep.2017.02.006

[19] M. R. Eid, O. D. Makinde. Solar radiation effect on a magneto nanofluid flow in a porous medium with chemically reactive species. *International Journal of Chemical Reactor Engineering* **16**(9):20170212, 2018.
https://doi.org/10.1515/ijcre-2017-0212

[20] S. Hazarika, S. Ahmed, A. J. Chamkha. Investigation of nanoparticles Cu, Ag and Fe_3O_4 on thermophoresis and viscous dissipation of MHD nanofluid over a stretching sheet in a porous regime: A numerical modeling. *Mathematics and Computers in Simulation* **182**:819–837, 2021.
https://doi.org/10.1016/j.matcom.2020.12.005

[21] M. D. Shamshuddin, A. Abderrahmane, A. Koulali, et al. Thermal and solutal performance of Cu/CuO nanoparticles on a non-linear radially stretching surface with heat source/sink and varying chemical reaction effects. *International Communications in Heat and Mass Transfer* **129**:105710, 2021. https://doi.org/10.1016/j.icheatmasstransfer.2021.105710

[22] M. C. Krishna Reddy, M. Gundagani, S. Sheri, N. V. N. Babu. Heat and mass transfer effects on unsteady MHD free convection flow past a vertical permeable moving plate with radiation. *International Journal of Applied Mathematical Research* **1**(2):189–205, 2012. https://doi.org/10.14419/ijamr.v1i2.45

[23] M. Gundagani, A. Paul, N. V. N. Babu. Heat and mass transfer effects on an unsteady hydromagnetic free convective flow over an infinite vertical plate embedded in a porous medium with heat absorption. *International Journal of Open Problems in Computer Science and Mathematics* **8**(1):15–27, 2015.
https://doi.org/10.12816/0010706

[24] D. Gadially, M. Gundagani. Analysis of soret and dufour effects on unsteady MHD convective flow past a semi-infinite vertical porous plate via finite difference method. *International Journal of Applied Physics and Mathematics* **4**(5):332–344, 2014.
https://doi.org/10.7763/IJAPM.2014.V4.306

[25] M. Gundagani, A. Paul, N. V. N. Babu. Numerical study of chemical reaction effects on unsteady MHD fluid flow past an infinite vertical plate embedded in a porous medium with variable suction. *Electronic Journal of Mathematical Analysis and Applications* **3**(2):179–192, 2015. https://doi.org/10.21608/ejmaa.2015.310762

[26] N. V. N. Babu, A. Paul, M. Gundagani. Soret and Dufour effects on unsteady hydromagnetic free convective fluid flow past an infinite vertical porous plate in the presence of chemical reaction. *Journal of Science and Arts* **1**(30):99–111, 2015.

[27] M. Gundagani, S. Sheri, N. V. N. Babu, M. C. Krishna Reddy. Finite element solution of thermal radiation effect on unsteady MHD flow past a vertical porous plate with variable suction. *American Academic & Scholarly Research Journal* **4**(3):3–22, 2012.

[28] N. V. N. Babu, M. Gundagani, S. M. Bhati. Casson fluid performance on natural convective dissipative couette flow past an infinite vertically inclined plate filled in porous medium with heat transfer, MHD and hall current effects. *International Journal of Pharmaceutical Research* **10**(4):809–819, 2018.

[29] M. Gundagani, S. Sheri, A. Paul, M. C. Krishna Reddy. Radiation effects on an unsteady MHD convective flow past a semi-infinite vertical permeable moving plate embedded in a porous medium with viscous dissipation. *Walailak Journal of Science and Technology* **10**(5):499–515, 2013.

[30] M. Gundagani, S. Sheri, A. Paul, M. C. Krishna Reddy. Unsteady magnetohydrodynamic free convective flow past a vertical porous plate. *International Journal of Applied Science and Engineering* **11**(3):267–275, 2013.

[31] M. Gundagani, D. Gadially, V. Nirmala Kasturi, P. K. Tanuku. Joint effects of thermal diffusion and diffusion thermo on MHD three dimensional nanofluid flow towards a stretching sheet. *Mathematical Models in Engineering* **9**(4):130–143, 2023. https://doi.org/10.21595/mme.2023.23590

[32] M. Gundagani, N. V. N. Babu, D. Gadially, et al. Study of Nano-Powell-Erying fluid flow past a porous stretching sheet by the effects of MHD, thermal and mass convective boundary conditions. *Journal of Umm Al-Qura University for Engineering and Architecture* **15**(3):271–281, 2024. https://doi.org/10.1007/s43995-024-00056-2

[33] M. Gundagani, L. P. Mamidi, P. K. Tanuku. Finite element solutions of double diffusion effects on three-dimensional MHD Nano-Powell-Erying fluid flow in presence of thermal and mass Biot numbers. *Journal of Engineering and Applied Science* **71**(1):9, 2024. https://doi.org/10.1186/s44147-023-00347-w

[34] D. Gadially, M. Gundagani. Effects of viscous dissipation on unsteady MHD free convective flow with thermophoresis past a radiate inclined permeable plate. *Iranian Journal of Science* **38**(3.1):379–388, 2014. https://doi.org/10.22099/ijsts.2014.2437

[35] S. A. A. Shah, N. A. Ahammad, E. M. T. E. Din, et al. Bio-convection effects on Prandtl hybrid nanofluid flow with chemical reaction and motile microorganism over a stretching sheet. *Nanomaterials* **12**(13):2174, 2022. https://doi.org/10.3390/nano12132174

[36] S. Nadeem, R. U. Haq, N. S. Akbar, Z. H. Khan. MHD three-dimensional Casson fluid flow past a porous linearly stretching sheet. *Alexandria Engineering Journal* **52**(4):577–582, 2013. https://doi.org/10.1016/j.aej.2013.08.005